Ultrarobust Wireless Interrogation for Sensors and Transducers: A Non-Hermitian Telemetry Technique

Minye Yang, Zhilu Ye, Mohamed Farhat, and Pai-Yen Chen, *Senior Member, IEEE*

***Abstract*— We herein introduce a non-Hermitian parity-time (PT)-symmetric telemetry platform, capable of wirelessly and robustly acquiring information of passive sensors and chemiresistive or piezoresistive transducers. We theoretically and experimentally demonstrate that the PT-symmetric radio frequency (RF) system, which consists of an active reader and a passive sensor to obey parity (space inversion) and time-reversal symmetries, may provide not only an improved sensitivity but also rapid, accurate, and robust acquisition of sensor data. The unidirectional reflectionless properties arising from the spontaneous PT symmetry-breaking may result in high-Q resonances and thus high resolvability in the measured reflection spectrum. Furthermore, the sensor's effective resistance (capacitance) can be wirelessly queried by electronically tuning the negative impedance converter (varactors) on the active reader, which allows observation of dual-band reflectionless phenomena. Unlike traditional telemetry systems, the measurement results are robust to the variations in the inductive coupling strength, namely, the distance and alignment between the two coil antennas. The proposed PT-symmetric telemetry paradigm may have an impact on a wide range of wireless sensing and instrumentation applications.**

***Index Terms*— Exceptional points (EPs), near-field probing, noninvasive measurement, parity-time (PT) symmetry, radio frequency (RF) sensors, telemetry instruments, wireless sensors.**

I. Introduction

5G AND beyond (5GB) wireless technologies provide wireless connectivity and continuous data gathering for a wide range of new applications in healthcare [1]–[4], vehicles [5], manufacturing industry [6], security [7], smart house automation [8], and Internet-of-Things (IoT) [9]–[11]. In general, wireless sensing technology can be categorized into active and passive telemetry [12]. Active sensor telemetry systems could provide relatively long-range bidirectional sensor data transmission, which comes at the price of increased size and shortened lifetime due to their internal batteries (power source). Passive (battery-free) sensor telemetry systems, although providing reduced transmission distances, enable indefinite lifetime and maintenance-free operation. Presently, there are two methods for implementing passive telemetry systems. One method is based on radio frequency identification (RFID) technology [10], [13]–[16], which monolithically integrates micromachined sensors with built-in signal conditioning units, analog-to-digital converters, and radio frequency (RF) backscatter onto a chip to reflect a modulated RF signal toward the reader located in the far zone. Another fully passive sensor telemetry approach, which could be lightweight, low-cost, and minimally invasive, is on the basis of *RLC*-oscillator-based sensors that are embedded or implanted in the system to be monitored. These structures can be readily fabricated using micromachining and/or printed circuit technology. In principle, the physical parameter of interest could tune the resonant frequency of the *RLC* sensor in the form of capacitive, resistive, or, less commonly, inductive perturbation. Hence, the loci of the resonant frequency drift can be monitored in a contactless way using a coil reader antenna inductively coupled to the *RLC* sensor. Wireless passive *RLC* sensors have been used for decades in monitoring of pressure [17], strain [18], food quality [19], temperature [20], environmental gases [21], and bacteria [22], for which the environmental parameter to be measured is encoded in the reflection spectrum (i.e., search of peak resonant frequency). In the past few decades, *RLC*-oscillator-based wireless sensors and actuators have been extensively studied in terms of device's structural design, fabrication, and cost reduction. Tremendous research effort has already been done in how to achieve the robust wireless readout. In fact, size/geometrical constrains of the sensor and measurement setup usually give rise to low sensitivity and spectral resolvability because the constraint of the quality factor is set by unavoidable skin effect, Eddy current, and/or dielectric losses. More critically, given that the resonant frequency shift has poor tolerance to misalignment between the sensor and reader coils in the both vertical and axial directions, absolute accuracy is sometimes questioned. A highly robust and accurate external readout circuit is thus an urgent demand for the practice of wireless *RLC* sensors. In this article, we will report a novel readout system for reliable and robust wireless query of passive *RLC* sensors, such as micromachined capacitive transducers [23], [24] or piezo-/chemi-resistive sensors [25], [26]. The proposed telemetry system is inspired

Manuscript received April 21, 2021; revised July 13, 2021; accepted August 5, 2021. Date of publication August 24, 2021; date of current version September 9, 2021. The work of Pai-Yen Chen was supported by the National Science Foundation under Grant ECCS-CCSS 1917678. The Associate Editor coordinating the review process for this article was Dr. Kamel Haddadi. *(Corresponding author: Pai-Yen Chen.)*

Minye Yang, Zhilu Ye, and Pai-Yen Chen are with the Department of Electrical and Computer Engineering, University of Illinois at Chicago, Chicago, IL 60607 USA (e-mail: pychen@uic.edu).

Mohamed Farhat is with the Computer, Electrical, and Mathematical Science and Engineering Division, King Abdullah University of Science and Technology (KAUST), Thuwal 23955, Saudi Arabia.

Digital Object Identifier 10.1109/TIM.2021.3107057

by parity-time (PT)-symmetric non-Hermitian Hamiltonians in quantum mechanics, which can be readily implemented and tested in electronic and electromagnetic systems with loss and/or gain. Our approach enables continuous real-time wireless readout of sensors, with absolute accuracy that is independent of the alignment and interrogation range between two coils, namely, a wireless telemetry system that does not require sophisticated alignment, tilt/range control, and collimation of coils during the interrogation process.

Ever since PT-symmetric quantum systems were discovered by Bender and Boettcher in 1998, there have been abundant studies in the exotic physical phenomenon [27]–[30]: non-Hermitian Hamiltonians may counterintuitively have entirely real eigenspectra once the system is invariant under combined operations of parity (P) and time-reversal (T) symmetry [27], [28]; the former operator is a linear operator performing spatial inversion to transform coordinates and momenta, whereas the latter operator is an antilinear operator conducing the time inversion. Given the antilinear character of PT, the Hamiltonian and the PT operator do not always share the same eigenvectors. As a matter of fact, beyond certain non-Hermiticity thresholds, abrupt phase transitions could occur, and the eigenvalues become complex. These spontaneous PT symmetry-breaking points are referred to as exceptional points (EPs), and their existence in non-Hermitian systems may lead to an interesting phenomenon of having both eigenvalues and eigenvectors converge simultaneously [27]–[30]. Although the concept of PT-symmetric quantum systems is still a matter of debate, its electromagnetic [31]–[34], optical [35]–[38], acoustic [39], and electronic analogs [40]–[46] have been experimentally demonstrated. Electronic and electromagnetic measurement systems, although seemingly unrelated to the quantum theory, exhibit formal similarities between the Helmholtz and Schrödinger equations, essentially originating from the isomorphism of the two equations, i.e., Helmholtz equation governs vector fields of a monochromatic electromagnetic wave, and the time-independent Schrödinger equation describes the wave function of a massive particle. Furthermore, electronic circuitry, which can be described by the telegraph equations (transmission line networks) and Kirchhoff's Laws (e.g., equivalence of wireless sensor telemetry and lumped-element circuitry), has emerged as a promising platform for observing PT symmetry and non-Hermitian physics because there are many experimentally feasible ways to create balanced, spatially modulated gain and loss in electronics [40]–[46].

In this context, we herein present theory and practical implementation for the PT-symmetric telemetric sensing system that enables flash and robust data acquisition. Fig. 1(a) and (b) illustrates the proposed PT-symmetric telemetry instrumentation and its practically realized circuit diagram for wireless interrogation of passive sensors and transducers, respectively. The circuit topologies in Fig. 2(a) and (b) can satisfy the PT-symmetry condition: the input impedances seen looking into either side have the same reactance and oppositely signed resistance of the same value, which is necessary for the time-reversal symmetry. Such a paired amplifying and attenuation oscillators wirelessly linked via inductive coupling

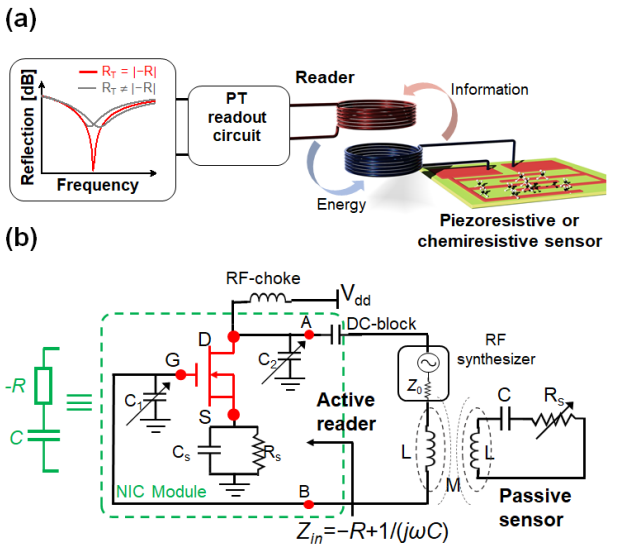

Fig. 1. (a) Schematics of the proposed PT-symmetric wireless measurement system where an active reader is configured to wirelessly interrogate a passive sensor or transducer through inductive coupling. (b) Equivalent circuit diagram for the PT-symmetric telemetry system in (a).

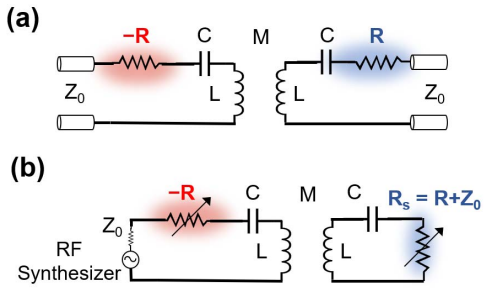

Fig. 2. (a) PT-symmetric electronic system realized with a two-port network. (b) Equivalent circuit model for the PT-symmetric wireless measurement system in Fig. 1; here, the active reader consisting of a coil antenna and an NIC is connected to a frequency synthesizer (e.g., VNA) with a generator impedance Z_0 to maintain PT-symmetry.

could support unidirectional reflectionless propagation for radio waves, when connected to a two-port network. The active resistance can be realized with the classical cross-coupled (XC) pair [47] with, for example, an input impedance of $-1/(2g_m)$ or a Colpitts-type feedback circuit [48]. For practical sensor telemetry applications, the active reader represents the $-RLC$ oscillator connected to the vector network analyzer (VNA) with a port impedance $Z_0 = 50\ \Omega$, while the passive sensor, typically modeled as an RLC oscillator, is terminated by a load resistance of Z_0 such that the PT-symmetry condition is valid, as illustrated in Fig. 2(b). In conventional passive sensing systems, the sensor information is generally encoded in the reflected signal, which can be amplitude and/or phase modulated by the effective impedance of RLC sensor. A straightforward way to read the sensor's impedance variations is to observe the shift in the resonance frequency. However, the resonance frequency is quite sensitive to the alignment between two coil antennas

because it could be readily shifted or split due to the changes in mutual inductance [49], [50]. On the other hand, in our approach, the sensor information is interpreted by the absolute value of $-R$ or C in the reader circuit, which enables rapid and precise contactless readout, with excellent lateral and vertical coil misalignment tolerances. In the following, we will present the theoretical foundation of PT-symmetric telemetric sensing technique in Section II, followed by experimental validation in Section III.

II. Theory of PT-Symmetric Telemetry

Based on Kirchhoff's law [51], [52] and assuming a time-harmonic field of the form $e^{j\omega t}$, the scattering matrix $\mathbf{S}$ of the two-port PT circuit sketched in Fig. 2(a) can be derived as

$$\mathbf{S} = \begin{bmatrix} t & r_R \\ r_L & t \end{bmatrix} = \frac{1}{a}\begin{bmatrix} jd & b - c_-^2 \\ b - c_+^2 & jd \end{bmatrix} \tag{1a}$$

$$a = b + j\frac{\omega^2 - 1}{\kappa\omega^2}d - c_+c_- \tag{1b}$$

$$b = Q^2\eta^2\left[\left(\kappa^2 - 1\right)\omega^4 + 2\omega^2 - 1\right] \tag{1c}$$

$$c_\pm = \omega(\eta \pm 1); \quad d = 2\eta Q\kappa\omega^3 \tag{1d}$$

where r_L and r_R are the reflection coefficients for the RF signal coming out of the left and right directions, respectively, and t is the transmission coefficient (which is independent of the direction of arrival of the incoming signals), the modified quality factor $Q = R^{-1}(L/C)^{1/2}$ (which can be seen as the non-Hermiticity of PT system), the coupling strength $\kappa = M/L$ where M is the mutual inductance between two coil antennas with a self-inductance L, $\eta = R/Z_0$, and ω is the angular frequency; here, all frequencies are measured in units of natural frequency $\omega_0 = 1/(LC)^{1/2}$. Since the system is reciprocal, $t_R = t_L = t$, and the product of two reflections is given by $r_R r_L^* = 1 - |t|^2$. In a typical passive network, flux conservation infers to the constraint $\mathbf{S}^\dagger(\omega)\mathbf{S}(\omega) = \mathbf{I}$, whereas in a PT-symmetric one, $\mathbf{S}$ in (1) satisfies $\mathcal{PT}\mathbf{S}^*(\omega)\mathcal{PT} = \mathbf{S}^{-1}(\omega)$ [36]. The transition between the exact PT-symmetric (exact PT) phase and broken PT-symmetric (PT-broken) phase can be identified by the asymptotic behavior of eigenvalues of $\mathbf{S}$ [36], given by

$$\lambda_\pm = t \pm \sqrt{r_R r_L} = \frac{jd \pm \sqrt{\left(b - c_+^2\right)\left(b - c_-^2\right)}}{2a}. \tag{2}$$

In the exact PT phase, the two eigenvalues are nondegenerate and unimodular ($|\lambda_\pm| = 1$), while the nonunimodular eigenvalues ($\lambda_+ = 1/(\lambda_-)^*$) suggest the PT-broken phase. At the EP, two eigenvalues are equal ($\lambda_+ = \lambda_- = 1/(\lambda_+)^*$); for further details about PT phase transition, see Appendix A. Fig. 3(a) presents evolution of eigenvalues as a function of Q and the normalized frequency ω; here, the coupling strength $\kappa = 0.6$. As can be clearly seen from Fig. 3(a), the PT phase transition is driven by the effective Q of the sensor and the frequency of operation. Fig. 3(b)–(d) presents the corresponding transmission coefficient (t) and the reflection coefficients (r_L and r_R) for the same system. It is seen from Fig. 3(a) and (b) that the change in the transmission coefficient from $|t| < 1$ to $|t| > 1$ is associated with the transition from the exact PT to PT-broken phase. Moreover, Fig. 3(b)–(d) clearly shows that the reflectionless perfect transmission occurs in one direction but not the other, at the EPs where unimodular eigenvalues would transit to nonunimodular ones. The EP frequencies can be derived from (2) as

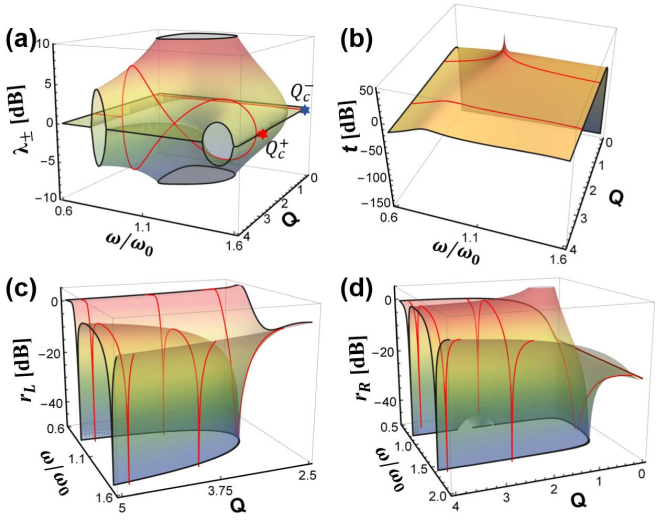

Fig. 3. (a) Contours of eigenvalues as functions of Q and ω for the electronic PT system in Fig. 2(a); here, $\kappa = 0.6$ and $\eta = 1.2$. The critical $Q_c^\pm$ are marked out by red and blue stars, respectively. (b)–(d) Corresponding transmission coefficient (t) and reflection coefficients at the left (r_L) and right (r_R) ports as functions of Q and ω for the PT system in (a).

$$\omega_{\mathrm{EP}}^{(1,2,3,4)} = \omega_0\sqrt{\frac{Q'^2 - 1 \pm \sqrt{1 - Q'^2 + 4Q'^4\kappa^4}}{2Q'^2(1 - \kappa^2)}} \tag{3}$$

where $Q' = [\eta/(1 + \eta)]Q$ and the "+" and "−" signs of Q' in (3) correspond, respectively, to two different types of unidirectional reflectionless propagation: 1) $r_L = 0$ and $r_R \neq 0$; and 2) $r_R = 0$ and $r_L \neq 0$; in both cases, $|t| = 1$. The zero-reflection effect could be attributed to the step-function-like behavior of the phase, which makes the delay time $\tau_{\mathrm{delay}} = \partial\arg(r)/\partial\omega$ behave as a delta function, and thus the reflected ac signals are trapped for a long time and completely absorbed by the loss element [53]. It is also observed from Fig. 3(a) that there exists a threshold Q value, beyond which real ω_{EP} can be found. The critical Q values can be derived as

$$Q_c^\pm = \frac{1 \pm (1/\eta)}{\kappa}\sqrt{\frac{1 \pm \sqrt{1 - \kappa^2}}{2}}. \tag{4}$$

If $Q \geq Q_c^+$, EPs with the first kind of unidirectional reflectionless propagation ($r_L = 0$) can be observed; Q_c^+ is marked as red star in Fig. 3(a). In the same vein, if $Q \geq Q_c^-$, the second kind of unidirectional reflectionless transmission ($r_R = 0$) can also be obtained [Q_c^- is marked with blue star in Fig. 3(a)]. Fig. 4(a) presents the evolution of eigenvalues of $\mathbf{S}$ as a function of the coupling strength κ and frequency ω; here, Q is fixed to 3. Those EPs observed in Fig. 4(a) can still be described by (3). The critical coupling strength that

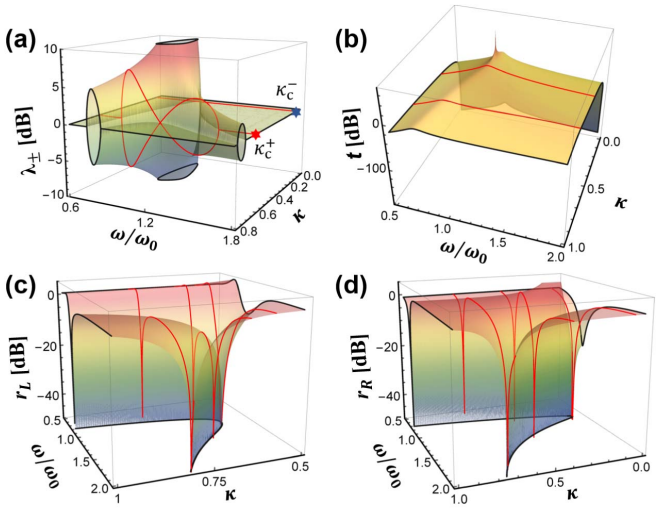

Fig. 4. (a) Contours of eigenvalues as functions of κ and ω for the electronic PT system in Fig. 2(a); here, $Q = 3$ and $\eta = 1.2$. The critical $\kappa_c^{\pm}$ are marked out by red and blue stars, respectively. (b)–(d) Corresponding transmission coefficient (t) and reflection coefficients from left (r_L) and right (r_R) as functions of κ and ω for the PT system in (a).

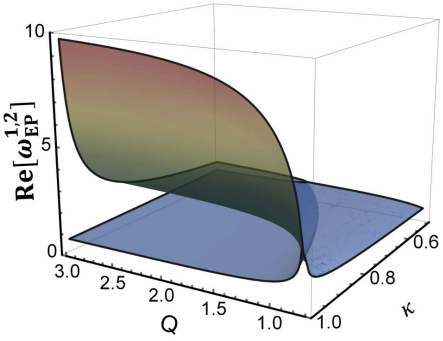

Fig. 5. Evolution of the normalized resonance frequencies (in unit of ω_0) as a function of Q and κ for the PT system in Fig. 2(a). There exist branch points at which the resonance frequencies shift drastically when Q or κ is varied.

enables the existence of real ω_{EP} can be derived as

$$\kappa_c^{\pm} = \frac{1 \pm (1/\eta)}{Q}\sqrt{1 - \left[\frac{1 \pm (1/\eta)}{2Q}\right]^2}. \tag{5}$$

If $\kappa \geq \kappa_c^+$, EPs with the first kind of unidirectional reflectionless property can be obtained. If $\kappa \geq \kappa_c^-$, another EP pair that leads to the second kind of unidirectional reflectionless event is also obtained. Fig. 4(b)–(d) reports the transmission and reflection coefficients for the system in Fig. 2(a), showing that the EP frequencies associated with the existence of (unidirectional) reflection dips can be well-described using (3) and (5). We should note that for a specific Q value, the magnetic coupling strength must be greater than κ_c, such that EPs and sharp resonances (dips) can be obtained in the reflection spectra. Equation (5) reveals that the interrogation distance between the reader and sensor coils must be sufficiently short if a low-Q oscillator is used. Fig. 5 shows $\omega_{\mathrm{EP}}^{(1,2)}$ as functions of Q and κ. It is seen from Fig. 5 that there are branch points at which ω_{EP} bifurcates and drastically varies with respect

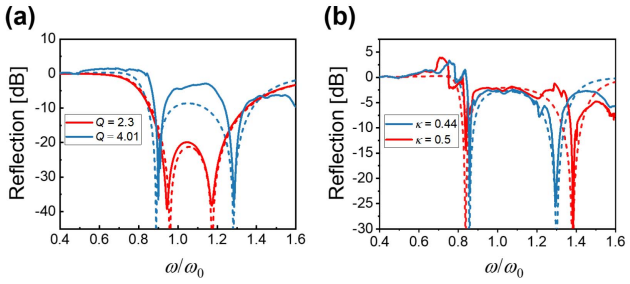

Fig. 6. (a) Reflection coefficients against frequency for different values of Q and $\kappa = 0.46$; here, the solid and dashed lines represent the experimental and theoretical results, respectively. (b) Similar to (a), but for different values of κ and $Q = 4.6$.

to the changes in Q and κ. Fig. 5 also presents the lower bound for (Q, κ) which allows observation of EPs and the associated sharp dips in the reflection spectra. Finally, we note that for a very small η, $Q'_+ \approx Q'_-$, and thus two different types of unidirectional reflectionless propagation could occur in the same frequency band. On the other hand, for a large η, the resonant frequencies of two different reflectionless scenarios are far apart.

For practical wireless sensing applications, a single port setup is usually adopted, as shown in Fig. 2(b), and the sensor's information is encoded solely in the reflection spectrum. Preferably, passive sensing apparatus comprising a coil antenna and a sensor or transducer may represent the loss element in the PT-symmetric telemetry system. In this case, the equivalent circuit model should be slightly modified as follows: the reader connected to the signal generator (generator impedance Z_0) has an effective negative resistance of $-R$, whereas the equivalent resistance of the sensor or transducer $R_s = R + Z_0$. This results in the PT-symmetry condition as illustrated in Fig. 2(b), namely, $|-R| = R = R_s - Z_0$, and the reactive/inductive elements in the sensor and the reader are identical. By doing so, the reflection of the system is the same as r_L obtained from the above two-port analysis. When Q is varied due to the changes in the resistance (capacitance) of the sensor, $-R(C)$ on the reader should be adjusted accordingly to maintain the PT-symmetry. Under a constant κ, the resistance variation (ΔR) or capacitance variation (ΔC) of the sensor can be characterized by tracking shifts of the two EP frequencies (i.e., loci of the two resonance frequencies), as shown in Fig. 6(a). This readout method, however, requisites delicate aligning and pitching between two coil antennas because ω_{EP} is rather sensitive to κ, as illustrated in Fig. 6(b). This represents the major challenge for the existing wireless passive LC sensor systems. In the proposed PT-symmetric telemetry system, for a given Q and an arbitrary κ, the analysis of ΔR (ΔC) of the sensor is done by reading the absolute $-R$ (C) value of the reader, instead of the κ (distance)-dependent resonance frequency shift. Thanks to the symmetry between the absolute resistance and reactance of the reader and the sensor, the sensor's ΔR (ΔC) can be contactlessly acquired by electronically sweeping $-R$ (C) of the reader until successful observation of two minima in the reflection spectrum (which means that two EPs are locked under the

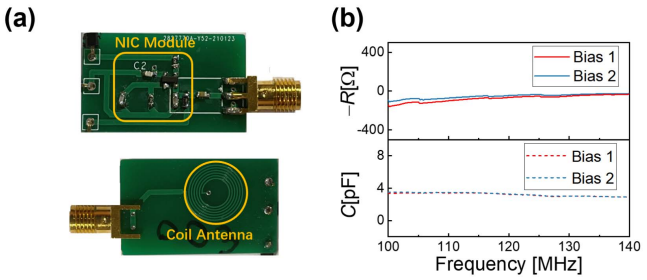

Fig. 7. (a) Photograph of the reader for the PT-symmetric telemetric sensing system in Fig. 1. (b) Retrieved equivalent negative resistance (solid line) and equivalent capacitance (dashed line) of the NIC at different bias voltages.

PT-symmetry condition). Since each (Q, κ) set corresponds to a unique EP frequency pair, the relationship between the measured resonance frequencies and the values of Q and κ could be obtained with proper interpolation.

Consequently, our approach may offer a rapid and accurate wireless measurement, which is robust to misalignment between the coil antennas or the variation in their separating distance, thus requiring no sophisticated alignments or positioning. On the other hand, conventional wireless sensing setups that rely on tracking the locus of impedance, phase, or peak frequency of a resonant mode do not provide similar absolute precision. There exists a general consensus that, to the best of the authors' knowledge, the data interpretation for the traditional wireless passive sensor system is complicated by the fact that two different sets of (Q, κ) could give the same resonance frequency. Additionally, traditional setups typically suffer from poor resolvability due to a rather broad spectral linewidth (low-Q resonance) [49], [54]. This, however, can be mitigated by the sharp reflectionless resonance in the electronic PT system.

III. Experiments and Discussions

We have conducted experiments for validating the proposed telemetric sensing method. In our laboratorial prototype, a reader and a pseudo-transducer were made using the printed circuit board (PCB) technology, as shown in Fig. 7(a). The self-inductance of the planar coil antenna and the mutual inductance between two coils can be determined by the Neumann formula [55]. In this work, the coil antenna self-inductance was designed to be $L = 200$ nH and the magnetic coupling coefficient is tuned from 0 to 0.5. We note that the coil antenna has a small parasitic resistance $R_p \approx 0.2\ \Omega$, retrieved from the scattering parameters. We have implemented a negative impedance converter (NIC) based on the Colpitts-type feedback oscillator shown in Fig. 1(b). In a Colpitts-type NIC, two variable shunt capacitors are connected parallel to the gate and drain terminals of a metal-oxide-semiconductor field-effect transistor (MOSFET; BF2040, fabricated by Infineon Inc.), as shown in Figs. 1(b) and 7(a). The input impedance seen in points A and B highlighted in Fig. 1(b) can be written as

$$Z_{\text{in}} = -R + \frac{1}{j\omega C} \approx -\frac{g_m(V_{\text{bias}})}{\omega^2 C_1 C_2} + \frac{1}{j\omega[C_1 C_2/(C_1 + C_2)]}. \quad (6)$$

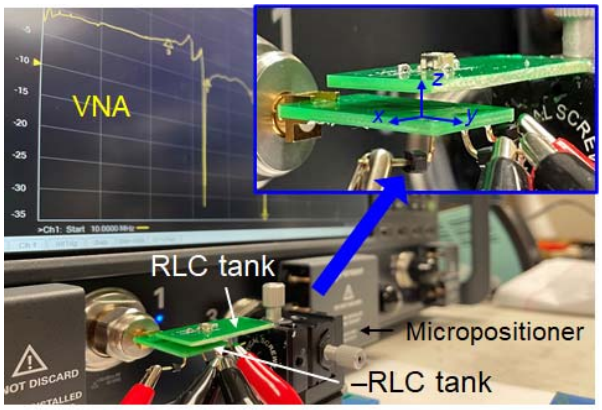

Fig. 8. Experimental setup of the PT-symmetric telemetric sensing system in Fig. 1, of which the active tank is directly connected to the VNA and the tunable passive tank as a pseudo-transducer is mounted on a micro positioner.

In (6), we assume that the transconductance $g_m \gg \omega C_{\text{gd}}$, ωC_{gs} (i.e., the operating frequency far below the cutoff frequency), where C_{gd} and C_{gs} represent the gate-to-drain capacitance and the gate-to-source capacitance, respectively. The NIC itself can be equivalent to a series combination of $-R$ and C seen in the joint points [points A and B in Fig. 1(b)]. Fig. 7(a) shows the prototype of the NIC and the active reader in Fig. 1(b), which were implemented using the PCB technology. By connecting the gate and drain of the MOSFET to the VNA and the planer coil antenna, a $-RLC$ tank can be constructed. We note that a VNA (N5242B, Keysight Technologies, Inc.) can be described by a negative resistance $-Z_0$ because it is regarded as an external source that steadily injects RF power to the system. Consequently, the net negative resistance of the active reader is $-R - Z_0$, which must be tuned to match the resistance of the passive sensor $R_s = R + Z_0$ such that the gain-loss balance, necessary for PT-symmetry, can be achieved. The negative resistance and the input reactance of an isolated $-RLC$ tank can be measured directly using the VNA. Fig. 7(b) reports the measured input impedance of the Colpitts-type NIC at different dc biases that tune $-R$ of the NIC, showing that a stabilized and rather nondispersive series negative resistance (with a bandwidth of $\sim$40 MHz) and an input capacitance can be achieved. Here, we note that different dc bias conditions may not lead to notable changes in the equivalent capacitance of the NIC module, as described in (6).

Fig. 8 illustrates our telemetry experiment setup where the active $-RLC$ reader and the passive RLC pseudo-transducer are inductively coupled to form the PT-symmetric electronic system in Fig. 1(a). Here, we used a variable resister in the RLC tank for mimicking a chemiresistive or piezoresistive transducer (PVG3A101C01R00 fabricated by Bourns Inc.). Fig. 6(a) and (b) reports the measured reflection coefficients for four different (Q, κ) sets, showing a good agreement between the experimental and theoretical results and proving validity and effectiveness of our reader circuit. In our experiment, the alignment and distance between two coil antennas is randomized. Under certain coupling strength, the exact

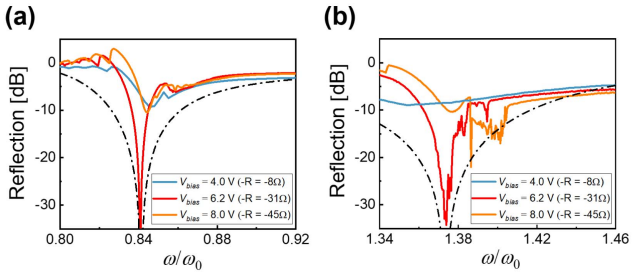

Fig. 9. (a) Reflection coefficients nearby (a) first and (b) second resonance frequency under different bias conditions; here, the black dash-dot lines are the theoretical results obtained from r_L (1). When the bias is tuned to 6.2 V, at which $|-R-Z_0| = R_s$, the reflection dips are obtained, in consistent with the theoretical prediction in (3) and Fig. 5.

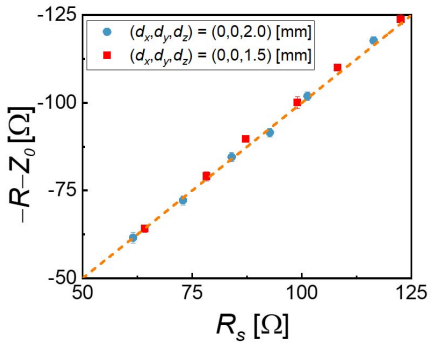

Fig. 10. Comparison between the measured and exact resistance of the pseudo-transducer achieved by a variable resistor.

Q and κ values can be extracted by adjusting the bias conditions of the MOSFET till observation of two reflection dips on the VNA screen, associated with unidirectional reflectionless property at ω_{EP} frequencies. Fig. 9(a) and (b) reports the variations in reflection coefficients around the two EP frequencies with different dc biases of the reader's NIC; here, $(Q, \kappa) = (4.7, 0.49)$, $R_s = 81\ \Omega$, $C = 2.3$ pF, and $L = 330$ nH. It can be seen from Fig. 9 that the first and second resonant dips are obtained when the bias is tuned to 6.2 V, which is in consistent with what was predicted by (3) (presented as the black dash-dot lines in Fig. 9). When the system is operating under the PT-symmetry condition, the two resonance frequencies [ω_1 and ω_2 in (3)] can be correlated with the unique set of (Q, κ). The effective resistance of the chemiresistor or piezoresistor is encoded in $Q \propto R^{-1}$.

Next, we intend to wirelessly read the resistance of the pseudo-transducer under an unknown coupling strength (distance) between the reader and sensor coils, to valid the robustness and reliability of this alignment-free telemetry system. Here, the resistance of the pseudo-transducer is known by manually adjusting the variable resistor. Fig. 10 reports the measurement results for two randomly selected coil-to-coil distances, respectively, represented by blue and red symbols. As mentioned above, under the condition of PT-symmetry, the sensor's effective resistance R_s must be equal to the sum of equivalent negative resistance of NIC $-R$ and the

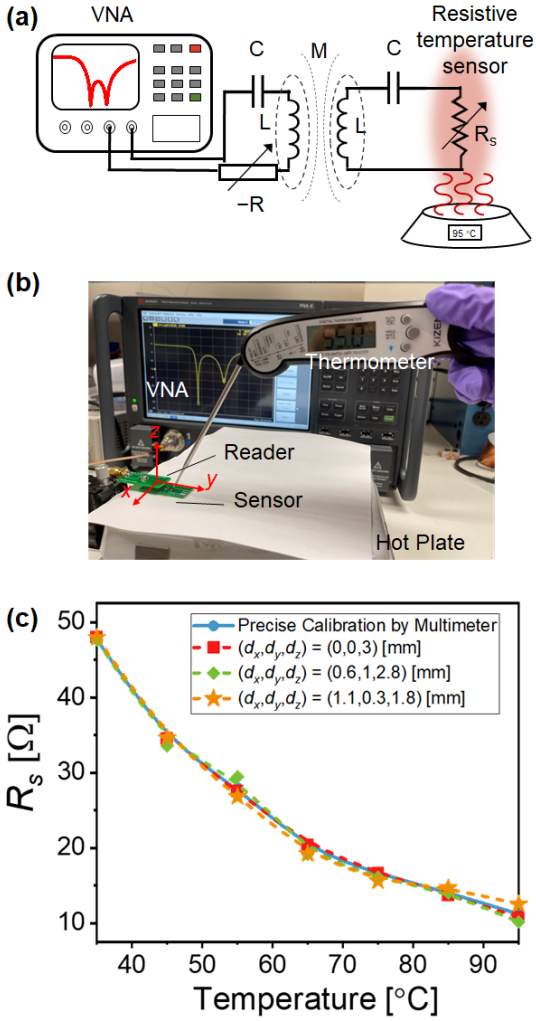

Fig. 11. (a) Schematic of the temperature sensing scenario using the PT telemetry system and an NTC resistor. (b) Realistic experimental setup of (a). (c) Measurement data points by the PT-telemetry system under different relative positions (d_x, d_y, d_z) between the sensor of two coil antennas with fitting lines.

negative resistance of the RF excitation source $-Z_0$ (e.g., 50 Ω for VNA used here). From Fig. 10, it is evident that the measurement results show excellent linearity, implying that the sensor's resistance value can be read in a contactless way with high accuracy by simply citing the negative resistance value of NIC, i.e., $|-R-Z_0| = R_s$. Finally, we present a wireless temperature sensor composed of the same coil antenna and capacitor in Fig. 9 and a negative temperature coefficient resistor (NTC resistor: NCP15XC680E03RC, Murata Electronics Inc.). The schematics and photograph of the wireless temperature sensing setup are shown in Fig. 11(a) and (b), respectively. The resistance of the sensor drops from 50 to 10 Ω when the substrate temperature increases from 35 °C to 95 °C. In our experiment, heat is generated from a hot plate in the laboratory. The relationship between the resistance of NTC resistor and the temperature is depicted by blue points in Fig. 11(c), which were obtained using the wired measurement with a digital multimeter. The red, green, and orange points in Fig. 11(c) are the results read wirelessly by the

proposed PT telemetry technique for different relative positions (d_x, d_y, d_z) between the center of two coil antennas. Each data point in Fig. 11(c) is the average result of the four measurements, with error bars representing the standard deviation of data. It can be evidently seen from Fig. 11(c) that accurate, repeatable, and reliable telemetry data acquisition can be accomplished, regardless of whether the coils are well-aligned. As a result, our telemetry technique provides a true alignment-free telemetric sensing, not possible with the traditional wireless *RLC* sensor systems [49], [50]. Although in this work we demonstrated a resistive sensing scheme, the proposed telemetry method can also be applied to reactive sensing schemes where a capacitive sensor is commonly used to tune the system's Q value (e.g., pressure and strain sensors [18], [56]). The accuracy can be further improved by optimizing the NIC design, e.g., implementation of NIC using complementary metal-oxide-semiconductor (CMOS) technology that can minimize noises and fabrication errors, thereby better controlling the effective $-R$ and C values. In addition to the precise control of resistive and reactive impedance values in the reader, the CMOS technology may also reduce the size and cost of readers and sensors, thus facilitating the practice of miniature wireless passive sensors in many applications. As representative examples, battery-free wireless *RLC* microsensors have been widely used in monitoring the human organ pressures, such as intraocular pressure [50], intracranial pressure [57], blood pressure [58], and intestine pressure [59], to name a few. These kinds of sensors are also commonly used in industry and automotive applications, such as the tire pressure monitoring system. Finally, wireless passive *RLC* sensors based on the low-temperature cofired ceramics (LTCC) substrate can operate in harsh (e.g., high temperature, toxic, and hazardous) environments [60], where wire connection may not be possible. The proposed telemetry technique is foreseen to be beneficial for these fields.

IV. Conclusion

We have proposed a robust, maker-free, and alignment-free telemetric sensing technique, inspired by PT-symmetry discovered first in Schrodinger and Helmholtz systems. In the non-Hermitian PT-symmetric telemetric sensing system requiring a subtle gain–loss balance, the unidirectional reflectionless property can be found at the EPs, associated with a unique set of the coupling strength and the quality factor of electronic oscillators (i.e., a passive *RLC* sensor and an active $-RLC$ reader, which are inductively or capacitively coupled). We demonstrate that at an arbitrary coil-to-coil distance (i.e., magnetic coupling strength), the changes in the effective impedance and Q-factor of an *RLC* sensor can be accurately and wirelessly read by sweeping bias voltages of the reader circuit and recording the values that give resonant reflection dips related to EPs. Once EPs are captured, the absolute value of reader's negative resistance (capacitance) determined by the bias voltage of NIC (varactor) should be identical to the effective resistance (capacitance) of the sensor, which is the condition imposed by PT-symmetry. Such telemetry approach does not require tracing the resonance frequency drift or amplitude/phase of the reflected signals at the resonant frequency, which are sensitive to both the effective impedance of the sensor and the inductive coupling strength. Hence, the proposed telemetry technique may address the long-standing problem encountered by the traditional wireless sensing systems, that is, the measurement results are very sensitive to the displacement and alignment of the reader antenna and, in general, the coil antennas must be precisely aligned and positioned. We envision that the proposed PT-symmetric telemetry technique may have an impact on the field of noninvasive and nondestructive wireless sensing for many real-world applications.

Appendix
Details on PT Phase Transition

In the two-port scattering problems, $\mathbf{S}$ has eigenvalues in (2) and the corresponding eigenvectors ψ_n, where $n \in \{1, 2\}$. Let ψ_n be an eigenvector of $\mathbf{S}$ corresponding to the eigenvalue λ_n, we may obtain the following relationship:

$$\mathbf{S}\mathcal{PT}\psi_n = \mathcal{PT}\left(\frac{1}{\lambda_n}\psi_n\right) \tag{A1}$$

$$\mathbf{S}(\mathcal{PT}\psi_n) = \frac{1}{\lambda_n^*}\mathcal{PT}\psi_n \tag{A2}$$

where it is clear that $\mathcal{PT}\psi_n$ is also an eigenvector of $\mathbf{S}$. Equation (A1) is a weaker constraint than unitarity and can be satisfied in two possible ways: either each eigenvalue is itself unimodular or the eigenvalues form pairs with reciprocal moduli, which correspond to the exact PT and PT-broken phases [37]. First, in the exact PT phase, $\mathcal{PT}$ and $\mathbf{S}$ share the same eigenvectors, that is, $\mathcal{PT}\psi_n = \pm\psi_n$. From (A1), we know that $\mathbf{S}(\pm\psi_n) = \pm\lambda_n\psi_n = \pm(\lambda_n^*)^{-1}\psi_n$, and therefore, $|s_n| = 1$. As a result, the spectrum of the $\mathbf{S}$ should be unimodular and nondegenerate. Physically, the eigenstate exhibits no net amplification or dissipation in the PT-exact phase [36]. Second, in the PT-broken phase, ψ_n is not PT-symmetric, but the eigenvectors satisfy $\mathcal{PT}$ by transforming into each other: $\mathcal{PT}\psi_n = \pm\psi_m$ and $n \neq m$. In such a phase, $\mathbf{S}(\pm\psi_n) = \pm(\lambda_n^*)^{-1}\psi_n$, and thus, $|\lambda_n||\lambda_m| = 1$. The eigenvalues of the $\mathbf{S}$ are nonunimodular and a complex conjugate reciprocal pair. Physically, one mode of the system is localized in the gain side, and thus exponentially amplified, while the other is localized in the loss side and thus dissipated. In other words, the eigenvectors of $\mathbf{S}$ cease to be PT-symmetric in the broken-PT phase. Finally, the third case occurs when the eigenvalues and eigenvectors of $\mathbf{S}$ are degenerate, namely, a transitional (exceptional) point which leads to spontaneously breaking of PT-symmetry. At the EP, the two eigenvectors become degenerate and so do their eigenvalues.

References

[1] Y.-D. Lee and W.-Y. Chung, "Wireless sensor network based wearable smart shirt for ubiquitous health and activity monitoring," *Sens. Actuators B, Chem.*, vol. 140, no. 2, pp. 390–395, 2009, doi: 10.1016/j.snb.2009.04.040.

[2] H. Huang, P.-Y. Chen, C.-H. Hung, R. Gharpurey, and D. Akinwande, "A zero power harmonic transponder sensor for ubiquitous wireless μL liquid-volume monitoring," *Sci. Rep.*, vol. 6, no. 1, May 2016, Art. no. 18795, doi: 10.1038/srep18795.

[3] H. Huang *et al.*, "RFID tag helix antenna sensors for wireless drug dosage monitoring," *IEEE J. Transl. Eng. Health Med.*, vol. 2, pp. 1–8, 2014, doi: 10.1109/JTEHM.2014.2309335.

[4] Y. Xu *et al.*, "Pencil–paper on-skin electronics," *Proc. Nat. Acad. Sci. USA*, vol. 117, no. 31, pp. 18292–18301, Aug. 2020, doi: 10.1073/pnas.2008422117.

[5] T. ElBatt, C. Saraydar, M. Ames, and T. Talty, "Potential for intra-vehicle wireless automotive sensor networks," in *Proc. IEEE Sarnoff Symp.*, Mar. 2006, pp. 1–4, doi: 10.1109/SARNOF.2006.4534723.

[6] W. Li and S. Kara, "Methodology for monitoring manufacturing environment by using wireless sensor networks (WSN) and the Internet of Things (IoT)," *Procedia CIRP*, vol. 61, pp. 323–328, Apr. 2017, doi: 10.1016/j.procir.2016.11.182.

[7] R. A. Potyrailo *et al.*, "Wireless sensors and sensor networks for homeland security applications," *TrAC Trends Anal. Chem.*, vol. 40, no. 4, pp. 133–145, Nov. 2012, doi: 10.1016/j.trac.2012.07.013.

[8] S. Pirbhulal *et al.*, "A novel secure IoT-based smart home automation system using a wireless sensor network," *Sensors*, vol. 17, no. 1, p. 69, 2016, doi: 10.3390/s17010069.

[9] S. Li, L. Da Xu, and X. Wang, "Compressed sensing signal and data acquisition in wireless sensor networks and Internet of Things," *IEEE Trans. Ind. Informat.*, vol. 9, no. 4, pp. 2177–2186, Nov. 2013, doi: 10.1109/TII.2012.2189222.

[10] L. Zhu, H. Huang, M. M.-C. Cheng, and P.-Y. Chen, "Compact, flexible harmonic transponder sensor with multiplexed sensing capabilities for rapid, contactless microfluidic diagnosis," *IEEE Trans. Microw. Theory Techn.*, vol. 68, no. 11, pp. 4846–4854, Nov. 2020, doi: 10.1109/TMTT.2020.3006286.

[11] H. Huang *et al.*, "Chemical-sensitive graphene modulator with a memory effect for Internet-of-Things applications," *Microsyst. Nanoeng.*, vol. 2, no. 1, Dec. 2016, Art. no. 16018, doi: 10.1038/micronano.2016.18.

[12] X. Xu, J. Wan, W. Zhang, C. Tong, and C. Wu, "PMSW: A passive monitoring system in wireless sensor networks," *Int. J. Netw. Manage.*, vol. 21, no. 4, pp. 300–325, Jul. 2011, doi: 10.1002/nem.792.

[13] C. Cattuto, W. Van den Broeck, A. Barrat, V. Colizza, J.-F. Pinton, and A. Vespignani, "Dynamics of person-to-person interactions from distributed RFID sensor networks," *PLoS ONE*, vol. 5, no. 7, Jul. 2010, Art. no. e11596, doi: 10.1371/journal.pone.0011596.

[14] L. Zhu, M. Farhat, Y.-C. Chen, K. N. Salama, and P.-Y. Chen, "A compact, passive frequency-hopping harmonic sensor based on a microfluidic reconfigurable dual-band antenna," *IEEE Sensors J.*, vol. 20, no. 21, pp. 12495–12503, Nov. 2020, doi: 10.1109/JSEN.2020.3000778.

[15] L. Zhu, N. Alsaab, M. M.-C. Cheng, and P.-Y. Chen, "A zero-power ubiquitous wireless liquid-level sensor based on microfluidic-integrated microstrip antenna," *IEEE J. Radio Freq. Identificat.*, vol. 4, no. 3, pp. 265–274, Sep. 2020, doi: 10.1109/JRFID.2020.3004351.

[16] K. Domdouzis, B. Kumar, and C. Anumba, "Radio-frequency identification (RFID) applications: A brief introduction," *Adv. Eng. Inform.*, vol. 21, no. 4, pp. 350–355, 2007, doi: 10.1016/j.aei.2006.09.001.

[17] B. Nie *et al.*, "Textile-based wireless pressure sensor array for human-interactive sensing," *Adv. Funct. Mater.*, vol. 29, no. 22, May 2019, Art. no. 1808786, doi: 10.1002/adfm.201808786.

[18] F. Stauffer *et al.*, "Soft electronic strain sensor with chipless wireless readout: Toward real-time monitoring of bladder volume," *Adv. Mater. Technol.*, vol. 3, no. 6, Jun. 2018, Art. no. 1800031, doi: 10.1002/admt.201800031.

[19] J. Koskela *et al.*, "Monitoring the quality of raw poultry by detecting hydrogen sulfide with printed sensors," *Sens. Actuators B, Chem.*, vol. 218, pp. 89–96, Oct. 2015, doi: 10.1016/j.snb.2015.04.093.

[20] S. Bhadra, D. S. Y. Tan, D. J. Thomson, M. S. Freund, and G. E. Bridges, "A wireless passive sensor for temperature compensated remote pH monitoring," *IEEE Sensors J.*, vol. 13, no. 6, pp. 2428–2436, Jun. 2013, doi: 10.1109/JSEN.2013.2255519.

[21] K. G. Ong, K. Zeng, and C. A. Grimes, "A wireless, passive carbon nanotube-based gas sensor," *IEEE Sensors J.*, vol. 2, no. 2, pp. 82–88, Apr. 2002, doi: 10.1109/JSEN.2002.1000247.

[22] K. G. Ong, J. Wang, R. S. Singh, L. G. Bachas, and C. A. Grimes, "Monitoring of bacteria growth using a wireless, remote query resonant-circuit sensor: Application to environmental sensing," *BioSens. Bioelectron.*, vol. 16, nos. 4–5, pp. 305–312, 2001, doi: 10.1016/S0956-5663(01)00131-2.

[23] B. T. Khuri-Yakub and Ö. Oralkan, "Capacitive micromachined ultrasonic transducers for medical imaging and therapy," *J. Micromech. Microeng.*, vol. 21, no. 5, May 2011, Art. no. 054004, doi: 10.1088/0960-1317/21/5/054004.

[24] I. Ladabaum, X. Jin, H. T. Soh, A. Atalar, and B. T. Khuri-Yakub, "Surface micromachined capacitive ultrasonic transducers," *IEEE Trans. Ultrason., Ferroelectr., Freq. Control*, vol. 45, no. 3, pp. 678–690, May 1998, doi: 10.1109/58.677612.

[25] A. S. Fiorillo, C. D. Critello, and A. S. Pullano, "Theory, technology and applications of piezoresistive sensors: A review," *Sens. Actuators A, Phys.*, vol. 281, pp. 156–175, Oct. 2018, doi: 10.1016/j.sna.2018.07.006.

[26] S.-W. Chiu and K.-T. Tang, "Towards a chemiresistive sensor-integrated electronic nose: A review," *Sensors*, vol. 13, no. 10, pp. 14214–14247, 2013, doi: 10.3390/s131014214.

[27] C. M. Bender and S. Boettcher, "Real spectra in non-hermitian Hamiltonians having PT dymmetry," *Phys. Rev. Lett.*, vol. 80, no. 24, pp. 5243–5246, Jun. 1998, doi: 10.1103/PhysRevLett.80.5243.

[28] C. M. Bender, D. C. Brody, and H. F. Jones, "Complex extension of quantum mechanics," *Phys. Rev. Lett.*, vol. 89, no. 27, Dec. 2002, Art. no. 270401, doi: 10.1103/PhysRevLett.89.270401.

[29] K. G. Makris, R. El-Ganainy, D. N. Christodoulides, and Z. H. Musslimani, "Beam dynamics in PT symmetric optical lattices," *Phys. Rev. Lett.*, vol. 100, no. 10, Mar. 2008, Art. no. 103904, doi: 10.1103/PhysRevLett.100.103904.

[30] R. El-Ganainy, K. G. Makris, D. N. Christodoulides, and Z. H. Musslimani, "Theory of coupled optical PT-symmetric structures," *Opt. Lett.*, vol. 32, no. 17, p. 2632, Sep. 2007, doi: 10.1364/OL.32.002632.

[31] R. Fleury, D. L. Sounas, and A. Alù, "Negative refraction and planar focusing based on parity-time symmetric metasurfaces," *Phys. Rev. Lett.*, vol. 113, no. 2, Jul. 2014, Art. no. 023903, doi: 10.1103/PhysRevLett.113.023903.

[32] B. Peng *et al.*, "Parity-time-symmetric whispering-gallery microcavities," *Nature Phys.*, vol. 10, pp. 394–398, Apr. 2014, doi: 10.1038/nphys2927.

[33] Z. Ye, M. Yang, L. Zhu, and P.-Y. Chen, "PTX-symmetric metasurfaces for sensing applications," *Frontiers Optoelectron.*, vol. 14, no. 2, pp. 211–220, Jun. 2021, doi: 10.1007/s12200-021-1204-6.

[34] M. A. K. Othman and F. Capolino, "Theory of exceptional points of degeneracy in uniform coupled waveguides and balance of gain and loss," *IEEE Trans. Antennas Propag.*, vol. 65, no. 10, pp. 5289–5302, Oct. 2017, doi: 10.1109/TAP.2017.2738063.

[35] C. E. Rüter, K. G. Makris, R. El-Ganainy, D. N. Christodoulides, M. Segev, and D. Kip, "Observation of parity-time symmetry in optics," *Nature Phys.*, vol. 6, no. 3, pp. 192–195, 2010, doi: 10.1038/nphys1515.

[36] L. Ge, Y. D. Chong, and A. D. Stone, "Conservation relations and anisotropic transmission resonances in one-dimensionalPT-symmetric photonic heterostructures," *Phys. Rev. A, Gen. Phys.*, vol. 85, no. 2, Feb. 2012, Art. no. 023802, doi: 10.1103/PhysRevA.85.023802.

[37] Y. D. Chong, L. Ge, and A. D. Stone, "PT-symmetry breaking and laser-absorber modes in optical scattering systems," *Phys. Rev. Lett.*, vol. 106, no. 9, Mar. 2011, Art. no. 093902, doi: 10.1103/PhysRevLett.106.093902.

[38] A. Regensburger, C. Bersch, M.-A. Miri, G. Onishchukov, D. N. Christodoulides, and U. Peschel, "Parity-time synthetic photonic lattices," *Nature*, vol. 488, no. 7410, pp. 167–171, 2012, doi: 10.1038/nature11298.

[39] R. Fleury, D. Sounas, and A. Alù, "An invisible acoustic sensor based on parity-time symmetry," *Nature Commun.*, vol. 6, p. 5905, Jan. 2015, doi: 10.1038/ncomms6905.

[40] M. Farhat, M. Yang, Z. Ye, and P.-Y. Chen, "PT-symmetric absorber-laser enables electromagnetic sensors with unprecedented sensitivity," *ACS Photon.*, vol. 7, no. 8, pp. 2080–2088, Aug. 2020, doi: 10.1021/acsphotonics.0c00514.

[41] M. Yang, Z. Ye, M. Farhat, and P.-Y. Chen, "Enhanced radio-frequency sensors based on a self-dual emitter-absorber," *Phys. Rev. A, Gen. Phys.*, vol. 15, no. 1, Jan. 2021, Art. no. 014026, doi: 10.1103/PhysRevApplied.15.014026.

[42] Y. Ra'Di *et al.*, "On-site wireless power generation," *IEEE Trans. Antennas Propag.*, vol. 66, no. 8, pp. 4260–4268, Aug. 2018, doi: 10.1109/TAP.2018.2835560.

[43] P.-Y. Chen *et al.*, "Generalized parity–time symmetry condition for enhanced sensor telemetry," *Nature Electron.*, vol. 1, no. 5, pp. 297–304, May 2018, doi: 10.1038/s41928-018-0072-6.

[44] M. Sakhdari, M. Hajizadegan, and P.-Y. Chen, "Robust extended-range wireless power transfer using a higher-order PT-symmetric platform," *Phys. Rev. Res.*, vol. 2, no. 1, Feb. 2020, Art. no. 013152, doi: 10.1103/PhysRevResearch.2.013152.

[45] Z. Ye, M. Yang, and P.-Y. Chen, "Multi-band parity-time-symmetric wireless power transfer systems," in *Proc. IEEE Wireless Power Transf. Conf. (WPTC)*, Jun. 2021, pp. 1–4, doi: 10.1109/WPTC51349.2021.9457925.

[46] M. Sakhdari, M. Hajizadegan, Y. Li, M. M.-C. Cheng, J. C. H. Hung, and P.-Y. Chen, "Ultrasensitive, parity–time-symmetric wireless reactive and resistive sensors," *IEEE Sensors J.*, vol. 18, no. 23, pp. 9548–9555, Dec. 2018, doi: 10.1109/JSEN.2018.2870322.

[47] T. Soorapanth and S. S. Wong, "A 0-dB IL 2140±30 MHz bandpass filter utilizing Q-enhanced spiral inductors in standard CMOS," *IEEE J. Solid-State Circuits*, vol. 37, no. 5, pp. 579–586, May 2002, doi: 10.1109/4.997850.
[48] J.-A. Hou and Y.-H. Wang, "A 7.9 GHz low-power PMOS colpitts VCO using the gate inductive feedback," *IEEE Microw. Wireless Compon. Lett.*, vol. 20, no. 4, pp. 223–225, Apr. 2010, doi: 10.1109/LMWC.2010.2042559.
[49] R. Nopper, R. Niekrawietz, and L. Reindl, "Wireless readout of passive LC sensors," *IEEE Trans. Instrum. Meas.*, vol. 59, no. 9, pp. 2450–2457, Sep. 2010, doi: 10.1109/TIM.2009.2032966.
[50] P.-J. Chen, S. Saati, R. Varma, M. S. Humayun, and Y.-C. Tai, "Wireless intraocular pressure sensing using microfabricated minimally invasive flexible-coiled LC sensor implant," *J. Microelectromech. Syst.*, vol. 19, no. 4, pp. 721–734, Aug. 2010, doi: 10.1109/JMEMS.2010.2049825.
[51] S. Tretyakov, *Analytical Modeling in Applied Electromagnetics*. Norwood, MA, USA: Artech House, 2003.
[52] D. M. Pozar, *Microwave Engineering*, 4th ed. Hoboken, NJ, USA: Wiley, 2012. [Online]. Available: https://search.library.wisc.edu/catalog/9910153599402121
[53] X. Zhu, H. Ramezani, C. Shi, J. Zhu, and X. Zhang, "PT-symmetric acoustics," *Phys. Rev. X*, vol. 4, no. 3, Sep. 2014, Art. no. 031042, doi: 10.1103/PhysRevX.4.031042.
[54] B. George, H. Zangl, T. Bretterklieber, and G. Brasseur, "A combined inductive–capacitive proximity sensor for seat occupancy detection," *IEEE Trans. Instrum. Meas.*, vol. 59, no. 5, pp. 1463–1470, May 2010, doi: 10.1109/TIM.2010.2040910.
[55] C. L. W. Sonntag, E. A. Lomonova, and J. L. Duarte, "Implementation of the Neumann formula for calculating the mutual inductance between planar PCB inductors," in *Proc. 18th Int. Conf. Electr. Mach.*, Sep. 2008, pp. 1–6, doi: 10.1109/ICELMACH.2008.4799978.
[56] Y. Peng, B. M. F. Rahman, T. Wang, G. Wang, X. Liu, and X. Wen, "Characterization of a passive telemetric system for ISM band pressure sensors," *J. Electron. Test.*, vol. 30, no. 6, pp. 665–671, Dec. 2014, doi: 10.1007/s10836-014-5485-1.
[57] N. H. Norager, A. Lilja-Cyron, T. S. Hansen, and M. Juhler, "Deciding on appropriate telemetric intracranial pressure monitoring system," *World Neurosurg.*, vol. 126, pp. 564–569, Jun. 2019, doi: 10.1016/j.wneu.2019.03.077.
[58] B. A. Ganji, S. Kheiry, and S. Soleimani, "Design of small size and high sensitive less-invasive wireless blood pressure sensor using MEMS technology," *IET Circuits, Devices Syst.*, vol. 13, no. 1, pp. 39–44, Jan. 2019, doi: 10.1049/iet-cds.2018.0013.
[59] P. Li, C. Kreikemeier-Bower, W. Xie, V. Kothari, and B. S. Terry, "Design of a wireless medical capsule for measuring the contact pressure between a capsule and the small intestine," *J. Biomech. Eng.*, vol. 139, no. 5, May 2017, Art. no. 051003, doi: 10.1115/1.4036260.
[60] J. Liu *et al.*, "Fiber-optic Fabry–Pérot pressure sensor based on low-temperature co-fired ceramic technology for high-temperature applications," *Appl. Opt.*, vol. 57, no. 15, p. 4211, May 2018, doi: 10.1364/AO.57.004211.

Minye Yang received the bachelor's degree in optical and electronic information from Huazhong University of Science and Technology, Wuhan, China, in 2018, and the M.Sc. degree in electrical engineering from Wayne State University, Detroit, MI, USA, in 2019. He is currently pursuing the Ph.D. degree in electrical engineering with the University of Illinois at Chicago, Chicago, IL, USA.

His research focuses on ultrasensitive electromagnetic sensors and RF/microwave circuits.

Zhilu Ye received the B.S. degree in microelectronics from Huazhong University of Science and Technology, Wuhan, China, in 2018, and the master's degree in electrical engineering from Arizona State University, Tempe, AZ, USA, in 2019. She is currently pursuing the Ph.D. degree with the University of Illinois at Chicago, Chicago, IL, USA.

Her research interest includes RF and microwave sensors, wireless communication, and wearable electronics.

Mohamed Farhat received the master's degree in theoretical physics and the Ph.D. degree in optics and electromagnetism from Aix-Marseille University, Marseille, France. His Ph.D. dissertation was entitled Metamaterials for Harmonic and Biharmonic Cloaking and Superlensing.

He is currently a Research Scientist with King Abdullah University of Science and Technology (KAUST), Thuwal, Saudi Arabia. He has authored over 170 publications, including one edited book, 85 journal articles, seven book chapters, five international patents, four proceedings, and over 70 conference papers, with over 4000 citations, as of August 2021. His research is in the fields of plasmonics and metamaterials with applications spanning optics and acoustics waves.

Dr. Farhat has organized several special sessions at META conferences, and is an Active Reviewer for many international journals in physics, including *Physical Review Letters* and *Nature Physics*. He has also co-edited the book *Transformation Wave Physics: Electromagnetics, Elastodynamics, and Thermodynamics* (Pan Stanford Publishing).

Pai-Yen Chen (Senior Member, IEEE) received the Ph.D. degree from The University of Texas at Austin, Austin, TX, USA, in 2013.

He was a Research Staff with the National Nano Device Laboratory, Hsinchu, Taiwan, from 2006 to 2009, and a Research Scientist with Intellectual Ventures' Metamaterial Commercialization Center, Bellevue, WA, USA, from 2013 to 2014. He is an Associate Professor with the Department of Electrical and Computer Engineering, University of Illinois at Chicago, Chicago, IL, USA. He has been involved in multidisciplinary research on applied electromagnetics, RF/microwave antennas and circuits, wireless micro/nanosensors and integrated systems, and nanoelectromagnetism in plasmonics and nanophotonics.

Dr. Chen was a recipient of a few prestigious awards, including the National Science Foundation (NSF) CAREER Award, the IEEE Sensors Council Young Professional Award, the IEEE Raj Mittra Travel Grant (RMTG) Award, the SPIE Rising Researcher Award, the ACES Early Career Award, the PIERS Young Professional Award, the Young Scientist Awards from URSI General Assembly and URSI Commission B: Electromagnetics, the IOP Measurement Science and Technology Emerging Leader, the Air Force Research Laboratory Faculty Fellowship, the National Argonne Laboratory Director's Fellowship, the College of Engineering Faculty Research Excellence Award, the Donald Harrington Fellowship, Taiwan Ministry of Education Study Abroad Award, and the United Microelectronics Corporation Scholarship, and quite a few student paper awards and travel grants from major IEEE conferences, including the USNC-URSI Ernest K. Smith Student Paper Award and Best Student Paper Award in Contest. He was a former Associate Editor of *Applied Electromagnetics*. He currently serves as an Associate Editor of the IEEE SENSORS JOURNAL, IEEE JOURNAL OF RADIO FREQUENCYIDENTIFICATION (IEEE JRFID), IEEE JOURNAL OF ELECTROMAGNETICS, RF AND MICROWAVES IN MEDICINE AND BIOLOGY (IEEE-JERM), and a Guest Editor of several international journals including IEEE TRANSACTIONS ON ANTENNAS AND PROPAGATION.